ACS APPLIED MATERIALS & INTERFACES

RESEARCH ARTICLE

www.acsami.org

Structural Transformation, Photocatalytic, and Field-Emission Properties of Ridged TiO_2 Nanotubes

Xijin Xu,[†,‡,*] Chengchun Tang,[§] Haibo Zeng,[‡] Tianyou Zhai,[*,‡] Shanqing Zhang,[*,†] Huijun Zhao,[†] Yoshio Bando,[‡] and Dmitri Golberg[*,‡]

[†]Environmental Futures Centre and Griffith School of Environment, Gold Coast Campus, Griffith University, QLD 4222, Australia,

[‡]International Center for Young Scientists (ICYS) and International Center for Materials Nanoarchitectonics (MANA), National Institute for Materials Science (NIMS), Namiki 1-1, Tsukuba, Ibaraki 305-0044, Japan,

[§]School of Materials Science and Engineering, Hebei University of Technology, Tianjin 300130, P. R. China

Supporting Information

ABSTRACT: Self-organized, freestanding TiO_2 nanotube arrays with ridged structures have been fabricated using a one-step anodic oxidation method. Their structural, photocatalytic, and field-emission (FE) properties have systematically been investigated. The as-synthesized nanostructures have been characterized using XRD, Raman spectroscopy, SEM, and HRTEM. The experimental results show that after an annealing process, the starting amorphous nanotubes have been turned into anatase phase structures, and the tube walls have been decorated with nanoparticles, different from the original ridged nanotubes. Furthermore, the anatase phase nanotubes have demonstrated better photocatalytic properties than their amorphous counterparts, which is caused by the larger surface area and improved crystallinity. With respect to FE properties, the as-grown nanotubes have the lower turn-on field E_{to} and the higher field enhancement factor β compared to the annealed nanotubes. The relationship between E_{to}, β, and the tube arrangements and morphologies has also been discussed.

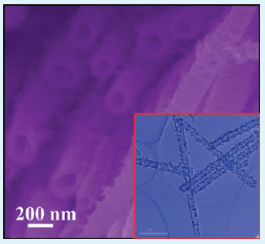

KEYWORDS: photocatalytic properties, field emission, TiO_2, semiconductors, nanotubes

Motivated by successful fabrication of porous alumina templates (PATs) that are widely used for the preparation of nanowires and nanotubes,[1−4] the anodization of metals such as tungsten,[5,6] niobium,[7,8] tantalum,[9] zirconium,[10] and iron[11] has intensively been studied to mimic the self-ordering phenomena displayed in PATs. Among various anodic porous metal oxides, titanium oxide (TiO_2) has attracted great attention due to its versatile applications, for example, in dye sensitized solar cells,[12] highly efficient photocatalytic devices,[13] ultrasensitive biosensors,[14] and biocompatible dental/bone implantations.[15]

Semiconductor photocatalysis has been widely investigated for potential applications in environmental pollutant degradation, water splitting, and photoelectric conversion.[16−18] TiO_2 nanotubes provide availability of their both internal and external areas for reactions, and they have been thought to be a decent material because of the enhanced surface areas. Although intensive research on the photocatalysis of 1D TiO_2 nanostructures has been carried out, the mechanisms on how the photocatalytic properties are affected by morphologies and crystallinity, being very important, have not yet been sufficiently explored.

In addition to the photocatalytic properties, we have investigated TiO_2 nanotubes with respect to their field-emission performance. Field emission (FE) is based on the physical phenomenon of quantum tunneling, during which electrons are injected from a material surface into vacuum under the influence of an applied electric field. Stimulated by the discovery of excellent FE performance of carbon nanotubes, much attention has been paid to explore the prospects of other 1D nanostructures as field emitters because of their low work functions, high aspect ratios, high mechanical stabilities, high conductivities, and so forth.[19] FE properties of TiO_2 nanowires have been reported by Wu et al.[20] and Xiang et al.;[21] and FE properties of TiO_2 nanotubes by hydrothermal-method fabrication and N-doped have also been studied.[22,23] However, studies on FE of pure TiO_2 nanotubes have still been rather limited presumably due to a limited success in reliable synthesis of conductive aligned nanotube arrays. It is well-known that FE properties mainly depend on the geometry (such as aspect ratio) and spatial distribution (such as alignment and density) of nanomaterials. Thus in the present work we have also investigated the morphology and arrangement dependence of FE properties of TiO_2 nanotubes.

Herein, we first show the formation of ridged TiO_2 nanotubes and discuss their growth mechanism, and then their structures and morphology transformations are analyzed. It is found that the nanotubes turn into an anatase phase from the amorphous state after an annealing process, and the annealed nanotubes become decorated with nanoparticle opposed to the starting ridged tube surfaces. The comparative photocatalytic and field emission properties of the nanotubes are also explored, and the results indicate that anatase nanotubes have far better photocatalytic properties than their amorphous counterparts, whereas the FE performance has an opposite trend.

Received: February 4, 2011
Accepted: March 28, 2011
Published: March 28, 2011

RESULTS AND DISCUSSION

SEM images in Figure 1 demonstrate the comparative morphologies of as-grown and annealed TiO_2 nanotube arrays, and the ridged structures are clearly seen for the as-grown nanotubes (Figure 1a–c). These arrays are uniform and compact, at least several micrometers in length (Figure 1a) and an outer tube diameter within the array is ~200 nm (Figure 1b and Figure 1c). The SEM images at a larger magnification (Figure 1b, c) distinctly show that the tubular ridged structures possess smooth inner surfaces. For the annealed ones, the outer surfaces of the tubes become coarse, as depicted in Figure 1d.

To improve crystallinity, we carried out thermal annealing process at 550 °C in air for 3 h. The corresponding X-ray diffraction patterns (XRD) shown in Figure S1 in the Supporting Information indicate that the as-prepared nanotube arrays are amorphous (red curve in Figure S1 in the Supporting Information), whereas they reveal an anatase phase after the heat treatment and the overall crystal structure becomes greatly refined (black curve in Figure S1 in the Supporting Information). The results are also confirmed by a Raman spectrum (see Figure S2 in the Supporting Information), in which a broad featureless plateau ranging from 100 to 1000 cm^{-1} is apparent (red curve in Figure S2 in the Supporting Information) for the as-prepared nanotube arrays, while the annealed nanotube arrays (black curve in Figure S2 in the Supporting Information) starts to show the specific peaks of anatase TiO_2 at 145, 198, 399, 516, and 640 cm^{-1}.[25,26] Such photoactive anatase phase[27] of the TiO_2 nanotubes is known to be preferable for use in dye-sensitized solar cells.

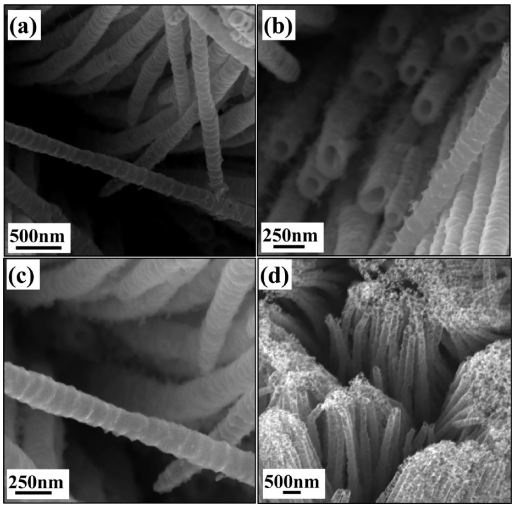

Figure 1. SEM images of ridged TiO_2 nanotubes at (a) low-magnification, and the corresponding enlarged (b) top-view and (c) side-view images for the as-grown nanotubes. (d) Low-magnification SEM image of annealed nanotubes.

Further insights into the effect of thermal treatment on the morphologies and structures of TiO_2 nanotube arrays were obtained during TEM and HRTEM observations. For the as-prepared TiO_2 nanotubes, the ridged surface structures are clearly visible in images a and b in Figure 2, and the FFT in Figure 2b indicates that the nanotubes are amorphous. However, the morphologies of the annealed nanotubes change into nanoparticle-decorated ones (Figure 2c, d and Figure S3a in the Supporting Information), and the ridged structure is not that evident as before. The nanoparticles are made of TiO_2, which can be confirmed by HRTEM imaging (see Figure S3b in the Supporting Information). The spacing between the lattice fringes for the nanoparticles decorated on the nanotubes is ca. 0.25 nm, corresponding to the JCPDS card No. 84–1284 of TiO_2. In some works,[34,61,62] the annealing effects on the morphology and structures have been observed, for example, Albu. et al.[34,62] have shown that until the annealing temperature becomes 450 °C the annealing process has converted the originally amorphous tubes entirely to anatase tubes.[62] The authors have also observed the formation of a double-walled structure in anodically grown TiO_2 nanotubes under a proper rapid thermal annealing process.[34] Furthermore, some nanocrystallites have also been found which build up the annealed nanotube walls.[34] The transformation to the TiO_2-nanoparticle-decorated morphology in our case may be caused by the unstability of an amorphous phase, governed by the nonequilibrium kinetics, abnormal speed of crystal growth, and the existence of the preferential crystal growth orientation. Thus the nanotubes recombine and lose

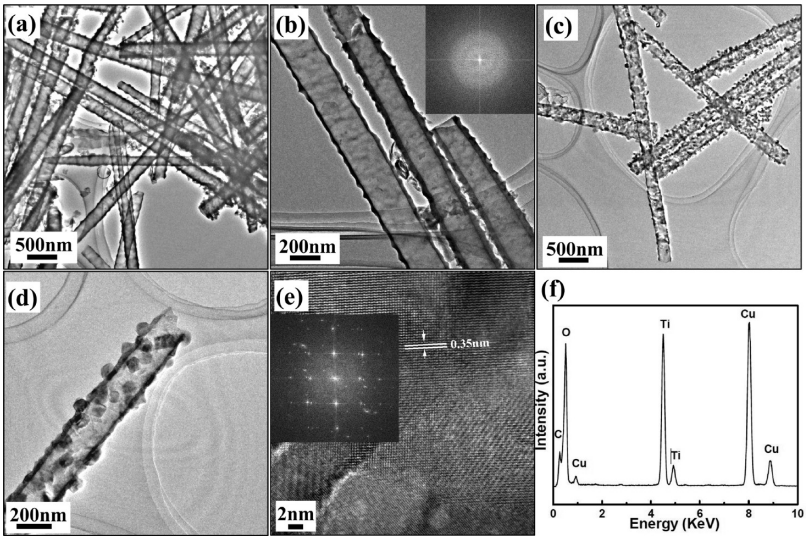

Figure 2. TEM images of ridged TiO_2 nanotubes: (a) TEM image, (b) enlarged TEM image and corresponding FFT pattern (inset) for the as-grown samples; and (c, d,) TEM and (e) HRTEM images and corresponding FFT patterns (inset) and (f) EDS spectrum of annealed nanotubes.

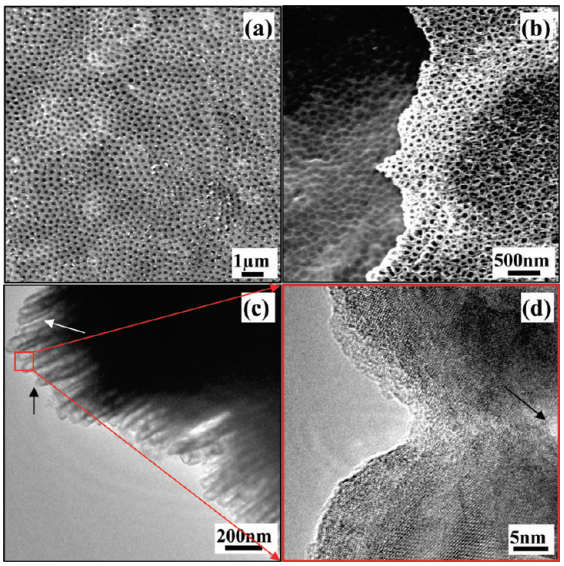

Figure 3. SEM images of (a) the surface pits at the electrolyte/oxide interface and (b) the nanopores at the early stage of anodization; (c) TEM image of TiO_2 nanotubes at the early stage of growth; (d) HRTEM image of conjunction between the two nanotubes.

their initial ridged structures, and the rapid growth of large crystals is accompanied with a fusion of the tubes into a TiO_2 nanoparticle-decorated structure during the annealing process. Furthermore, the annealed nanotubes become crystalline, as confirmed by the HRTEM and FFT images in Figure 2e. The spacing between the lattice fringes is *ca* 0.35 nm, which is well indexed as [101] zone axis lattice orientation of an anatase TiO_2 crystal, according to the JCPDS card No. 21−1272. An EDS spectrum shown in Figure 2f further confirms the ultimate chemical purity of the TiO_2 nanotubes, only Ti and O peaks are visible.

Chemical reactions during Ti anodization are complex and many efforts have been paid to study the formation mechanism and the related as-anodized morphologies.[28−30] The as-anodized products generally have a smooth one-walled morphology, furthermore, many different morphologies such as dot-like structures, double-walled nanotubes, bamboo-type nanotubes, tube-in-tube (TIT) nanotubes and nanowires have also been realized by adjusting experimental conditions, such as electrolyte type or applied votages.[24,31−36] For the formation mechanism, it is commonly accepted that the process includes field assisted oxidation of Ti to form TiO_2, field-assisted dissolution of Ti metal ions in the electrolyte and chemical dissolution of Ti and TiO_2 due to etching by fluoride ions and hydrogen ions.[24,28] For the formation mechanism of ridged nanotubes, Figure S4 in the Supporting Information shows the current changes (I−t curves) recorded during the anodization process; the initial drastic current drop is due to the formation of a compact oxide film at the initial stage which elevates the resistance and reduces current densities. The barrier layer of TiO_2 forms on the metal surface when Ti is anodized, and many pits are formed on the surface (Figure 3a) at this stage. With the extension of the anodization time, the current densities start to increase in the later stages (shown as Figure S4 in the Supporting Information) and pores start to grow randomly because of the dissolution of titanium oxide, which is accompanied with a competition between the growing pores, and the current densities start to decrease again, until a stable, ordered pore growth is

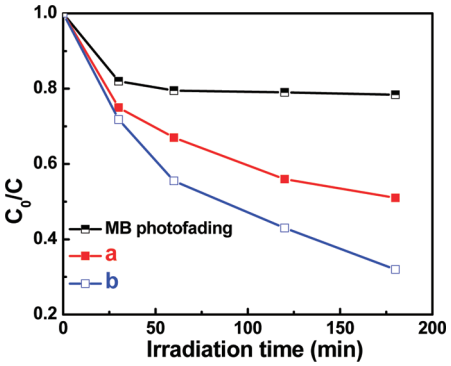

Figure 4. Photodegradation efficiency of MB: (a) as-grown amorphous ridged TiO_2 nanotubes and (b) annealed anatase nanoparticle-decorated TiO_2 nanotubes. (The black line for the MB photofading is selected from ref 24 for comparison.)

established. The nanopores are developed from these pits, as shown in Figure 3b. It is apparent that the nanotubes are protruding out of these pits. Thanks to our previous experiments on TIT nanotubes,[24] we know that in addition to the growth of one nanotube at the bottom (downward), the pore diameter also expands until the two nanotubes touch each other, which can be also confirmed from the TEM image in Figure 3c. From this image one may realize that in addition to connected nanotubes (as indicated in Figure 3c with a black arrow), some nanotubes are clearly separated into two portions (as indicated in Figure 3c with a white arrow). Because the hydroxide layer exists,[24] the formation mechanism of these ridged nanotubes can be ascribed to be volume contraction, which has also been taken into account for the explanation of O-rings nanotubes by Zhou's group.[28] Because of the electric field and local-heating-enhanced dehydration, the nanotubes are able to separate from each other as elucidated in Figure 3c, where the direction of volume contraction of the hydroxide layer is normal to the walls. Besides that, the contraction direction caused by the field can also be in the growth direction of the nanotubes.[28] The electric field at the pore base between the two neighboring tubes could be divided into the parallel and normal directions, leading to a volume contraction along and perpendicular to the tube wall. The effect of the parallel contraction will induce small cracks in more condensed oxide between nanotubes as the black arrow indicates in Figure 3d. This shows that the two nanotubes are connected, and herein the ridged nanotubes are formed being caused by the parallel contraction.

Titanium dioxide has attracted a lot of interest because of its unique photoinduced reactivity explored for applications in environmental photocatalysis, solar energy conversion, and the more recently discovered effect of light-induced amphiphilicity. Pollutants can be degraded by TiO_2 under both UV and visible light illuminations, when it is combined with a dopant, such as methylene blue (MB),[37−40] gaseous toluene,[41] methyl orange,[42,43] amaranth,[44] and phenol.[45] The photocatalytic activities of the present samples have been evaluated by measuring the degradation of MB in an aqueous solution under UV light irradiation. Figure 4 shows the effects of annealing process and the morphologies on the photocatalytic degradation of MB. It is obvious that the annealing process and the morphologies have a strong influence on the nanotube photoactivity. The photocatalytic activities increase after annealing, i.e., the crystalline nanotubes have a stronger photocatalytic activity than the amorphous samples. In the photocatalytic

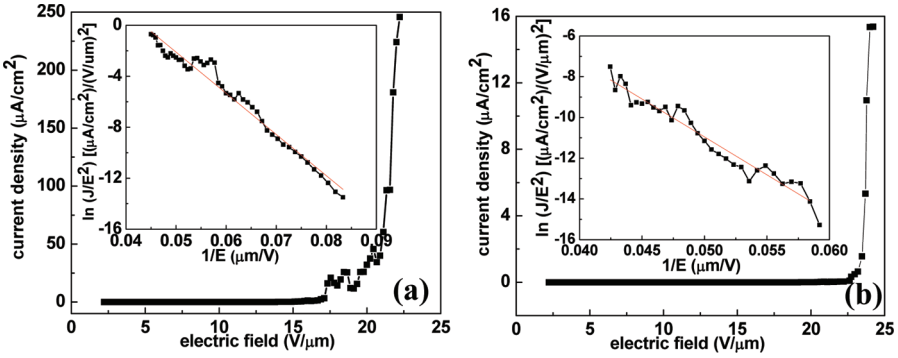

Figure 5. Field-emission properties of (a) as-grown amorphous ridged and (b) annealed anatase nanoparticle-decorated TiO_2 nanotubes (at a working distance of 45 μm). The insets are the corresponding Fowler−Nordheim plots showing the linear dependences.

reaction, an anatase phase and the surface area dominate the main effect.[46−48] When the nanotubes are annealed, the amorphous TiO_2 gradually turns into the anatase TiO_2, and such crystallization raises the photocatalytic activity. Furthermore, besides the effect of crystallization, the transformation of the morphology also improves the photocatalytic activity, because the as-formed TiO_2 nanoparticles decorated on the tube surfaces should inevitably increase the surface area of the tubular nanostructures. This is the key point for the photocatalytic performances. Furthermore, as reported by other groups,[49−53] when the TiO_2 nanotubes are sensitized by elements or compound nanoparticles, the photocatalytic activity can be greatly improved. This is coincident with our observations. Thus the collective effects of the improved crystallinity and the increased surface area induce better photocatalytic performance for the annealed nanoparticle-decorated nanotubes compared with as-prepared amorphous ones, as summarized in Figure 4.

The FE current−voltage characteristics of TiO_2 nanotubes are analyzed by the Flower-Nordheim (F−N) equation[54,55]

$$J = (A\beta^2E^2/\phi)\exp(-B\phi^{3/2}/\beta E) \quad (1)$$

$$\text{or } \ln(J/E^2) = \ln(A\beta^2/\phi) - B\phi^{3/2}/\beta E \quad (2)$$

where A and B are constants with values of 1.54×10^{-6} A eV V^{-2} and 6.83×10^3 V μm^{-1} $eV^{-3/2}$, respectively, J is the current density, β is the field enhancement factor, E is the applied field, and ϕ is the work function of the emitting materials (6.79 eV for TiO_2[56]). Generally, the values of β are related to the emitter geometry (such as aspect ratios), crystal structure, vacuum gaps and the spatial distribution of emitting centers.[57] The linear variation of $\ln(J/E^2)$ with $1/E$ (F−N plot), as shown in the insets in Figure 5, supports the hypothesis that the current is due to field emission, according to the F−N theory. From the slope of the linear part of the F−N plot and using ϕ, β can be calculated.

Figure 5 shows the room temperature FE measurements on nanotubes with different morphology and crystallinity performed in a high-vacuum chamber (1.7×10^{-6} Pa). A distance between the anode and the tips of the TiO_2 nanowires was 45 μm. The emission current density J exponentially increases with an increase of the applied field E. Herein, we define the turn-on field (E_{to}) as the electronic field required to produce a current density of 10 μAcm^{-2}. According to the calculation, we can deduce that compared to the annealed tubes the as-prepared nanotubes have the lower E_{to} values (the numbers are 17.2 and 23.8 Vμm^{-1} for the amorphous and anatase tubes, respectively) and the higher β values (373 and 324 for the amorphous and anatase nanotubes, respectively). Many factors can affect the electron emission properties of nanostructured TiO_2. It is very difficult to determine the exact contribution of each factor and their possible relevance. However, it is generally accepted that the crystallinity, the arrangements and the surface states of the wire or tube arrays,[22,23] are the key issues for the FE properties, and the competition between these factors finally dominates the final FE performances. Generally, the better crystallinity and the alignment can endow the TiO_2 semiconductors better FE performances. In our case, the anatase phase shows lower electron emission compared with the amorphous phase (Figure 5), which can be ascribed to the regarded morphology transformation. According to the morphologies' characterization, we understand that when the nanotubes are annealed, they are changed into nanoparticle-decorated structures which lead to higher E_{to}. From the eq 1, parameters that govern the emission are the material effective work function ϕ and geometric enhancement factor β. The latter describes how the electric fields can be enhanced by protrusions from the emitting surface, which is related to the emitter geometry (such as the aspect ratio), crystal structure, and the spatial distribution of emitting centers. It has been reported that the field emission performance of nanostructures, such as Ge[54] nanowires and ZnO[58] nanobelts, can be significantly enhanced through decreasing the density of the nanowires and increasing the aspect ratio (length-to-thickness ratio). Then, the decreased geometric enhancement factor β for the annealed nanoparticle-decorated nanotubes can be ascribed to the poorer arrangements and decreased aspect ratios because of surface morphology transformation.

To assess the dependence of the FE properties on the distances between the anodes and the samples, the FE measurements were additionally performed at various distances d between the aluminum anode and the tube array. Figure 6 shows the FE current density, J, as a function of the applied field, E, for a $J-E$ plot (Figure 6a) and a $\ln(J/E^2) - (1/E)$ plot (Figure 6b) measured at the anode−cathode distances of 10, 15, 20, and 25 μm, respectively, for the annealed nanotubes. The F−N plots are presented in Figure 6b and the F−N curves are basically fitted to lines within the measurement range, so the emission is indeed attributed to a vacuum tunneling process, that is, the field emissions still follow the F−N law. When the distance increases from 10 to 25 μm, the E_{to} decreases monotonously from 96.2 to 34 Vμm^{-1} during a voltage increase. From the slope of the linear part of the F−N plot, β can be calculated to be 61.8, 115.6, 214.2, and 255.5 for d = 10, 15, 20, and 25 μm, respectively. The linear behavior, Figure 6c, in the increment of distance d from 10 to 25

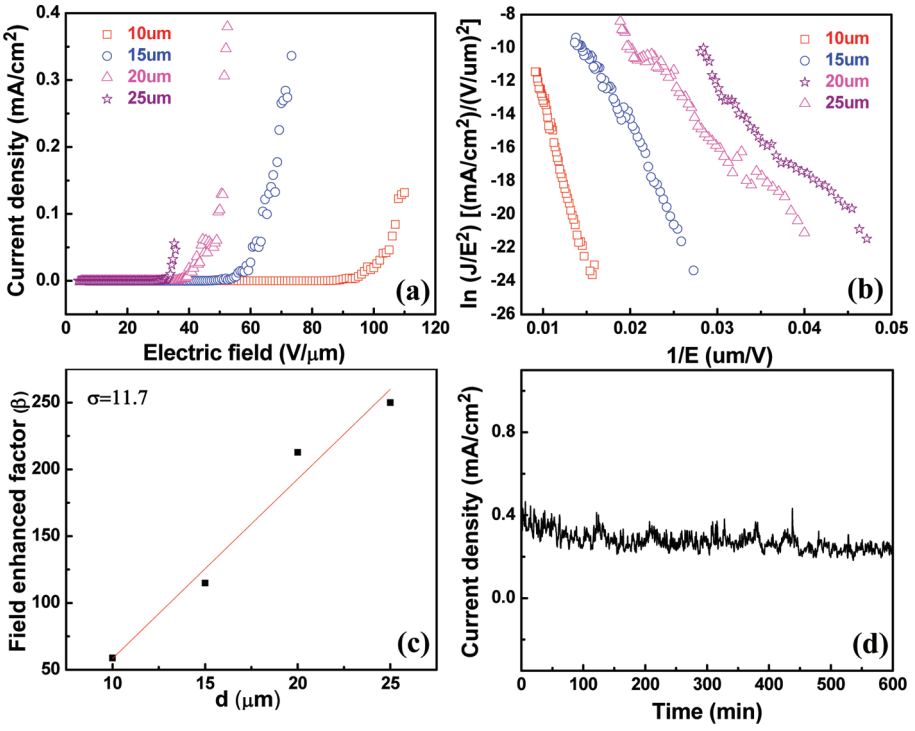

Figure 6. (a) $J-E$ plots and (b) corresponding F−N plots for nanoparticle-decorated TiO_2 nanotubes at a different sample-anode separation, d; (c) the variation in field enhancement factor (β) with a distance (d); (d) stable emission current recorded from ridged nanotubes.

μm, is consistent with the literature[59] and our previous report on CdS nanowires.[60] A FE stability measurement was performed on the as-grown ridged TiO_2 nanotubes by keeping the electric field at 100 V μm^{-1}. No dramatic fluctuation or degradation was observed for the emission current over a period of 600 min, as illustrated in Figure 6(d). The current fluctuated between 0.23 and 0.29 mA cm^{-2} and was relatively stable during the entire measurement. Since the current fluctuations were lower than 10%, it suggests the high stability of the present TiO_2 nanotube emitters. Furthermore, the emission current density exceeded 0.26 mA cm^{-2}, which is higher than the previously reported values of 0.15 $mAcm^{-2}$.[22] The stable FE performance shown in this work is related to the uniform height of the TiO_2 nanotubes within the arrays, which guarantees a uniform field distribution across the structures. Good emission stability demonstrates that the present TiO_2 nanotubes could find potential applications in the cold-cathode-based electronics.

CONCLUSION

In summary, we have reported the formation of self-organized, free-standing TiO_2 nanotube arrays with ridged structures using the one-step anodic method. The as-grown TiO_2 nanotubes are amorphous but crystallize into the photoactive anatase form after annealing at 550 °C in air. The surface morphology of the ridged TiO_2 nanotubes changes into the nanoparticle-decorated ones after the annealing process. Both photocatalytic activities and FE properties have been studied to the correlate them with the tube morphologies and structures. The results show that the nanoparticle-decorated nanotubes possess better photocatalytic activity than the as-prepared counterparts, which can be ascribed to the larger surface area and improved crystallinity caused by the annealing process. FE measurements verify that the alignments of TiO_2 nanotubes have a prime effect on their stimulated emission, the better the alignments for the as-prepared ridged nanotubes, the lower the turn-on field E_{to} and the higher β as compared to the annealed nanoparticle-decorated nanotubes. The established relationship between the field enhancement factor, turn-on field and the tube arrangements, and morphologies sheds an additional light on their FE mechanism. Good emission stability demonstrates that TiO_2 nanotubes could find potential application in the cold-cathode-based electronics.

METHODS

The fabrication method for the TiO_2 nanotubes was similar to that described in our previous report.[24] In brief, an as-cut Ti foil was pretreated with a series of cleaning processes, and then immersed in the mixture of 2% HF and DMSO, which was used as the supporting electrolyte. Electrochemical anodization was carried out using a DC power at a constant potential of 40 V for 56 h, with a platinum foil served as the counter electrode. After the anodization process, in order to improve the crystallinity, the TiO_2 nanotubes were annealed in air, under ramping the temperature to 550 °C in 2 h and holding for 3 h.

A scanning electron microscope (SEM, JSM-6700F), a transmission electron microscope (HRTEM, JEM-3000F) equipped with an X-ray energy dispersive spectrometer (EDS), an X-ray diffractometer (XRD, Shimadzu 6000 X-ray diffractometer, Cu K_α radiation, λ = 1.5406 Å) and a Raman spectrometer (Raman, Horiba Jobin-Yoon T6400) were used for the product characterizations.

For the photocatalytic activity evaluation, the organic dyes (primal solution: 1.0×10^{-5} M, 30 mL) and the catalysts (10 mg) were thoroughly stirred in the dark to reach the adsorption equilibrium of the organic dyes with the catalyst and then

exposed to a UV light (125 W). The concentration of photodegraded methylene blue (MB) was monitored using a spectrophotometer (SP-2000UV).

The FE properties were studied at room-temperature (25 °C) in a high vacuum chamber ($1-2 \times 10^{-6}$ Pa) using an aluminum anode with cross-sectional area of 1 mm^2. A dc voltage sweeping from 100 to 1100 V was applied to the samples with a voltage step of 10 V and a delay time of 2 s.

■ ASSOCIATED CONTENT

Supporting Information. XRD (Figure S1) and Raman spectra (Figure S2) of as-grown amorphous (red curve) and anatase (black curve) TiO_2 nanotubes. Figure S3 shows the TEM image of a nanotube and the HRTEM image of a nanoparticle. Figure S4 shows $I-t$ curve at a constant voltage during the anodizing process and Figure S5 presents the $J-E$ plots and corresponding F−N plots for as-grown TiO_2 nanotubes at a different sample-anode separation, d; manifesting the variations of the field enhancement factor (β) with a distance (d). This material is available free of charge via the Internet at http://pubs.acs.org.

■ AUTHOR INFORMATION

Corresponding Author

*E-mail: x.xu@griffith.edu.au, xu.xijin@yahoo.com (X.X.); zhai.tianyou@gmail.com (T.Z.); s.zhang@griffith.edu.au (S.Z.); GOLBERG.Dmitri@nims.go.jp (D.G.).

■ ACKNOWLEDGMENT

This work was supported by Griffith University, Australia, and the World Premier International Center for Materials Nanoarchitectonics (MANA) of the National Institute for Materails Science (NIMS). H.B.Z. thanks the Japan Society for Promotion of Science (JSPS) for a support in the form of a fellowship tenable at the National Institute for Materials Science (NIMS), Tsukuba, Japan.

■ REFERENCES

(1) Masuda, H.; Fukuda, K. *Science* **1995**, *268*, 1466–1468.
(2) Jessensky, O.; Maller, F.; Gösele, U. *J. Electrochem. Soc.* **1998**, *145*, 3735–3740.
(3) Choi, J; Sauer, G.; Nielsch, K.; Wehrspohn, R. B.; Gösele, U. *Chem. Mater.* **2003**, *15*, 776–779.
(4) Steinhart, M.; Wendorff, J. H.; Greiner, A.; Wehrspohn, R. B.; Nielsch, K.; Schilling, J.; Choi, J.; Gösele, U. *Science* **2002**, *296*, 1997.
(5) Mukherjee, N.; Paulose, M.; Varghese, O. K.; Mor, G. K.; Grimes, G. A. *J. Mater. Res.* **2003**, *18*, 2296–2299.
(6) Tsuchiya, H.; Macak, J. M.; Sieber, I.; Taveira, L.; Ghicov, A.; Sirotna, K.; Schmuki, P. *Electrochem. Commun.* **2005**, *7*, 295–298.
(7) Sieber, I.; Hildebrand, H.; Friedrich, A.; Schmuki, P. *Electrochem. Commun.* **2005**, *7*, 97–100.
(8) Choi, J.; Lim, J. H.; Kim, K. J.; Lee, S. C.; Chang, J. H.; Cho, M. A. *Electrochim. Acta* **2006**, *51*, 5502–5507.
(9) Sieber, I.; Kannan, B.; Schmuki, P. *Electrochem. Solid-State Lett.* **2005**, *8*, J10–J13.
(10) Tsuchiya, H.; Schmuki, P. *Electrochem. Commun.* **2004**, *6*, 1131.
(11) Prakasam, H. E.; Varghese, O. K.; Paulose, M.; Mor, G. K.; Grimes, C. A. *Nanotechnology* **2006**, *17*, 4285–4291.
(12) Mor, G. K.; Shankar, K.; Paulose, M.; Varghese, O. K.; Grimes, C. A. *Nano Lett.* **2006**, *6*, 215–218.
(13) Livraghi, S.; Votta, A.; Paganini, M. C.; Giamello, E. *Chem. Commun.* **2005**, 498–500.
(14) Rajh, T.; Saponjic, Z.; Liu, J. Q.; Dimitrijevic, N. M.; Scherer, N. F.; Vega-Arroyo, M.; Zapol, P.; Curtiss, L. A.; Thurnauer, M. C. *Nano Lett.* **2004**, *4*, 1017–1023.
(15) Sul, Y. T.; Johansson, C. B.; Petronis, S.; Krozer, A.; Jeong, Y.; Wennerberg, A.; Albrektsson, T. *Biomaterials* **2002**, *23*, 491.
(16) Linsebigler, A. L; Lu, G.; Yates, T. J. *Chem. Rev.* **1995**, *95*, 735–738.
(17) Kavan, L.; Grätzel, M.; Gilbert, S. E.; Klemenz, C.; Scheel, H. J. *J. Am. Chem. Soc.* **1996**, *118*, 6716–6723.
(18) Leng, W. H.; Liu, H.; Cheng, S. A.; Zhang, J. Q.; Cao, C. N. *J. Photochem. Photobiol. A* **2000**, *131*, 125–132.
(19) Fang, X. S.; Gautam, U. K.; Bando, Y.; Dierre, B.; Sekiguchi, T.; Golberg, D. *J. Phys. Chem C* **2008**, *112*, 4735–4742.
(20) Wu, J. M.; Shih, H. C.; Wu, W. T. *Chem. Phys. Lett.* **2005**, *413*, 490–494.
(21) Xiang, B.; Zhang, Y.; Wang, Z.; Luo, X. H.; Zhu, Y. W.; Zhang, H. Z.; Yu, D. P. *J. Phys. D: Appl. Phys.* **2005**, *38*, 1152.
(22) Miyauchi, M.; Tokudome, H.; Toda, Y.; Kamiy, T.; Hosono, H. *Appl. Phys. Lett.* **2006**, *89*, 043114.
(23) Liu, G.; Li, F.; Wang, D. W.; Tang, D. M.; Liu, C.; Ma, X.; Lu, G. Q.; Cheng, H. M. *Nanotechnology* **2008**, *19*, 025606.
(24) Xu, X.; Fang, X.; Zhai, T.; Zeng, H.; Liu, B.; Hu, X.; Bando, Y.; Golberg, D. *Small* **2011**, *7*, 445–449.
(25) Varghese, O. K.; Gong, D. W.; Paulose, M.; Ong, K. G.; Dickey, E. C.; Grimes, C. A. *Adv. Mater.* **2003**, *15*, 624–627.
(26) Wang, J.; Lin, Z. *Chem. Mater.* **2008**, *20*, 1257–1261.
(27) Varghese, O. K.; Gong, D. W.; Paulose, M.; Grimes, C. A.; Dickey, E. C. *J. Mater. Res.* **2003**, *18*, 156–165.
(28) Su, Z.; Zhou, W. *J. Mater. Chem.* **2009**, *19*, 2301–2309.
(29) Mor, G. K.; Varghese, O. K.; Paulose, M.; Mukherjee, N.; Grimes, C. A. *J. Mater. Res.* **2003**, *18*, 2588–2593.
(30) Su, Z.; Zhou, W. *Adv. Mater.* **2008**, *20*, 3663–3667.
(31) Lim, J. H.; Choi, J. *Small* **2007**, *3*, 1504–1507.
(32) Kim, S. E.; Lim, J. H.; Lee, S. C.; Nam, S. C.; Kang, H. G.; Choi, J. *Electrochim. Acta* **2008**, *53*, 4846–4851.
(33) Choi, J.; Wehrspohn, R. B.; Lee, J.; Gösele, U. *Electrochim. Acta* **2004**, *49*, 2645–2652.
(34) Albu, S. P.; Ghicov, A.; Aldabergenova, S.; Drechsel, P.; LeClere, D.; Thompson, G. E.; Macak, J. M.; Schmuki, P. *Adv. Mater.* **2008**, *20*, 4135.
(35) Albu, S. P.; Kim, D.; Schmuki, P. *Angew. Chem., Int. Ed.* **2008**, *47*, 1916.
(36) Macak, J. M.; Tsuchiya, H.; Schmuki, P. *Angew Chem. Int. Ed.* **2005**, *44*, 2100–2102.
(37) Gu, D.; Lu, Y.; Yang, B.; Hu, Y. *Chem. Commun.* **2008**, 2453–2455.
(38) Lin, C.; Yu, W.; Lu, Y.; Chien, S. *Chem. Commun.* **2008**, 6031–6033.
(39) Zhang, X.; Pan, J. H.; Du, A. J.; Lee, P. F.; Sun, D. D.; Leckie, J. O. *Chem. Lett.* **2008**, *37*, 424–425.
(40) Wang, D.; Hu, T.; Hu, L.; Yu, B.; Xia, Y.; Zhou, F.; Liu, W. *Adv. Funct. Mater.* **2009**, *19*, 1930–1938.
(41) Wu, Z.; Dong, F.; Zhao, W.; Wang, H.; Liu, Y.; Guan, B. *Nanotechnology* **2009**, *20*, 235701.
(42) Yang, L.; Luo, S.; Liu, S.; Cai, Q. *J. Phys. Chem. C* **2008**, *112*, 8939–8943.
(43) Tafen, D. N.; Wang, J.; Wu, N.; Lewis, J. P. *Appl. Phys. Lett.* **2009**, *94*, 093101–3.
(44) Qamar, M.; Kim, S. J.; Ganguli, A. K. *Nanotechnology* **2009**, *20*, 455703.
(45) Wu, Y.; Long, M.; Cai, W.; Dai, S.; Chen, C.; Wu, D.; Bai, J. *Nanotechnology* **2009**, *20*, 185703.
(46) Wang, Y.; Wang, Y.; Meng, Y.; Ding, H.; Shan, Y.; Zhao, X.; Tang, X. *J. Phys. Chem. C* **2008**, *112*, 6620–6226.
(47) An, H.; Zhu, B.; Li, J.; Zhou, J.; Wang, S.; Zhang, S.; Wu, S.; Huang, W. *J. Phys. Chem. C* **2008**, *112*, 18772–18775.
(48) Wang, J.; Li, R. H.; Zhang, Z. H.; Zhang, X. D.; Sun, W.; Wang, H.; Xu, R.; Xing, Z. Q. *J. Chem. Technol. Biotechnol.* **2007**, *82*, 588–597.
(49) Mohapatra, S. K.; Kondamudi, N.; Banerjee, S.; Misra, M. *Langmuir* **2008**, *24*, 11276–11281.

(50) Awazu, K.; Fujimaki, M.; Rockstuhl, C.; Tominaga, J.; Murakami, H.; Ohki, Y.; Yoshida, N.; Watanabe, T. *J. Am. Chem. Soc.* **2008**, *130*, 1676–1680.
(51) Baker, D. R.; Kamat, P. V. *Adv. Funct. Mater.* **2009**, *19*, 805–811.
(52) Zhu, R.; Jiang, C. Y.; Liu, B.; Ramakrishna, S. *Adv. Mater.* **2009**, *21*, 994–1000.
(53) Bavykin, D. V.; Friedrich, J. M.; Walsh, F. C. *Adv. Mater.* **2006**, *18*, 2807–2824.
(54) Li, L.; Fang, X. S.; Chew, H. G.; Zheng, F.; Liew, T. H.; Xu, X. J.; Zhang, Y. X.; Pan, S. S.; Li, G. H.; Zhang, L. D. *Adv. Funct. Mater.* **2008**, *18*, 1080–1088.
(55) Fang, X. S.; Bando, Y.; Ye, C. H.; Golberg, D. *Chem. Commun.* **2007**, 3048–3050.
(56) Vogtenhuber, D.; Podloucky, R.; Neckel, A.; Steinemann, S. G.; Freeman, A. J. *Phys. Rev. B* **1994**, *49*, 2099–2103.
(57) Gautam, U. K.; Fang, X. S.; Bando, Y.; Zhan, J. H.; Golberg, D. *ACS Nano* **2008**, *2*, 1015.
(58) Wang, W. Z.; Zeng, B. Q.; Yang, J.; Poudel, B.; Huang, J. Y.; Naughton, M. J.; Ren, Z. F. *Adv. Mater.* **2006**, *18*, 3275–3278.
(59) Xu, Z.; Bai, X. D.; Wang, E. G. *Appl. Phys. Lett.* **2006**, *88*, 133107.
(60) Zhai, T.; Fang, X.; Bando, Y.; Dierre, B.; Liu, B.; Zeng, H.; Xu, X.; Huang, Y.; Yuan, X.; Sekiguchi, T.; Golberg, D. *Adv. Funct. Mater.* **2009**, *19*, 2423–2430.
(61) Ghicov, A.; Tsuchiya, H.; Macak, J. M.; Schmuki, P. *Phys. Stat. Sol. (a)* **2006**, *203*, R28–R30.
(62) Albu, S. P.; Tsuchiya, H.; Fujimoto, S.; Schmuki, P. *Eur. J. Inorg. Chem.* **2010**, 4351–4356.